Personalizing oral delivery of nanoformed piroxicam by semi-solid extrusion 3D printing

Mathiyalagan, Rathna; Sjöholm, Erica; Manandhar, Sajana; Lakio, Satu; Rosenholm, Jessica M.; Kaasalainen, Martti; Wang, Xiaoju; Sandler, Niklas

Published in:
European Journal of Pharmaceutical Sciences

DOI:
https://doi.org/10.1016/j.ejps.2023.106497

Published: 01/09/2023

Document Version
Final published version

European Journal of Pharmaceutical Sciences 188 (2023) 106497

Contents lists available at ScienceDirect

European Journal of Pharmaceutical Sciences

journal homepage: www.elsevier.com/locate/ejps

Personalizing oral delivery of nanoformed piroxicam by semi-solid extrusion 3D printing

Rathna Mathiyalagan [a], Erica Sjöholm [a], Sajana Manandhar [b], Satu Lakio [b], Jessica M. Rosenholm [b], Martti Kaasalainen [b,1,*], Xiaoju Wang [a,1,*], Niklas Sandler [a,b]

[a] Pharmaceutical Sciences Laboratory, Faculty of Science and Engineering, Åbo Akademi University, Tykistökatu 6A, 20520 Turku, Finland
[b] Nanoform Finland Ltd, Viikinkaari 4, 00790 Helsinki, Finland

ARTICLE INFO

Keywords:
Poorly water-soluble drug
Drug nanoparticles
Semi-solid extrusion 3D printing
Personalized medicine
Nanoforming
Drug delivery

ABSTRACT

Semi-solid extrusion (SSE) 3D printing enables flexible designs and dose sizes to be printed on demand and is a suitable tool for fabricating personalized dosage forms. Controlled Expansion of Supercritical Solution (CESS®) is a particle size reduction technology, and it produces particles of a pure active pharmaceutical ingredient (API) in a dry state, suspendable in the printing ink. In the current study, as a model API of poorly water-soluble drug, nanoformed piroxicam (nanoPRX) prepared by CESS® was accommodated in hydroxypropyl methylcellulose- or hydroxypropyl cellulose-based ink formulations to warrant the printability in SSE 3D printing. Importantly, care must be taken when developing nanoPRX formulations to avoid changes in their polymorphic form or particle size. Printing inks suitable for SSE 3D printing that successfully stabilized the nanoPRX were developed. The inks were printed into films with escalating doses with exceptional accuracy. The original polymorphic form of nanoPRX in the prepared dosage forms was not affected by the manufacturing process. In addition, the conducted stability study showed that the nanoPRX in the prepared dosage form remained stable for at least three months from printing. Overall, the study rationalizes that with nanoparticle-based printing inks, superior dose control for the production of personalized dosage forms of poorly water-soluble drugs at the point-of-care can be achieved.

1. Introduction

A current hurdle in drug delivery is that approximately 90% of drugs in development are poorly water-soluble, which complicates the drug development and may very likely result in poor bioavailability (Loftsson and Brewster, 2010). Improving the bioavailability of drugs is often challenging, but it is commonly known that a drug's dissolution rate is associated with its particle size. Hence, particle size reduction is a rational way to address this issue. When the size of a drug particle is decreased, the specific surface area increases, resulting in an increased dissolution rate that can lead to enhanced bioavailability with a faster onset of action. Apart from current micronizing techniques, several particle engineering technologies have been utilized to enhance poorly water-soluble drugs' solubility, bioavailability, and dissolution rate (Savjani et al., 2012), such as nanoforming or nanoparticle engineering technology (Lakio and Sandler, 2020). Piroxicam (PRX) is a nonsteroidal anti-inflammatory drug, under the class of oxicam, which is used to reduce pain, swelling, and joint stiffness caused by arthritis. It is a commercially available drug with poor aqueous solubility (0.023 mg/mL) (Shohin et al., 2014), and its oral absorption is limited by its dissolution rate. Controlled Expansion of Supercritical Solutions (CESS®) is a new technology used to improve the dissolution of poorly soluble drugs. In nanoparticle engineering, the precise control of the nucleation and crystal growth is critical, and the CESS® technology is based on supercritical carbon dioxide (sc-CO_2) extraction with bottom-up control to the crystallization process. Additional benefits of the CESS® technology are that it produces dry state drug nanoparticles without requiring excipients or organic solvents (Pessi et al., 2016). In this study, CESS®-produced nanosized piroxicam (nanoPRX) was used as a model drug in the fabrication of oral dosage forms *via* semi-solid extrusion (SSE) 3D printing.

Conventional tablets are manufactured on a large scale with uniform sizes according to the concept of one-size-fits-all. In contrast to conventional tableting, (3D) printing technology offers flexible dosage

* Corresponding authors.
E-mail addresses: martti.kaasalainen@nanoform.com (M. Kaasalainen), xiaoju.wang@abo.fi (X. Wang).
[1] Equally contributed authors at Pharmaceutical Sciences Laboratory and Nanoform Finland Ltd.

https://doi.org/10.1016/j.ejps.2023.106497
Received 17 March 2023; Received in revised form 26 May 2023; Accepted 14 June 2023
Available online 16 June 2023

forms for individual patients by simple adjustment of the design. Many researchers and the pharmaceutical industry have generated interest towards 3D printing after the first 3D-printed dosage form Spritam, an orodispersible tablet produced by Aprecia Pharmaceuticals using their ZipDose® technology, received the Food and Drug Administration (FDA) approval in 2015 (Eisenstein, 2015). In recent years, 3D printing has made an impact in the pharmaceutical industry by the development of personalized medicinal products (Trenfield et al., 2018; Jamróz et al., 2018). Due to its adaptable, innovative, and versatile applications, additive manufacturing or 3D printing technologies have been explored in different systems for use in the biomedical, healthcare, and pharmaceutical fields (Shahrubudin et al., 2019; Vaz and Kumar, 2021). In recent years, many studies have explored the printing of nanoparticles using different 3D printing technologies for pharmaceutical applications. Chou et al. fabricated drug-eluting 3D printed screws loaded with vancomycin hydrochloride and ceftazidime hydrate filled with polycaprolactone/nano-hydroxyapatite nanocomposites using solution-based extrusion 3D printing (Chou et al., 2021). Isoniazid-containing pharmaceutical 3D-printed oral dosage forms with a novel ferromagnetic nanoparticle as an excipient using selective laser sintering 3D printing were produced by Zhang et al. (2021). Mirdamadian et al. printed oxaliplatin-loaded alginate nanoparticles to produce 3D-printed tablets using hot-melt extrusion (HME) and fused deposition modeling (FDM) 3D printing (Mirdamadian et al., 2022). FDM 3D printing was used by Topsakal et al. to develop 3D-printed polyvinyl alcohol-based gold nanoparticle scaffolds loaded with ampicillin for tissue engineering (Topsakal et al., 2021). Liu et al. developed fish-gelatin-based hydrogel patches containing PEGylated liposomal doxorubicin nanomedicine by 3D bio-printing (Liu et al., 2020). When not including cells in the bioink, bio-printing is referred to as SSE 3D printing and this technique is currently being explored to produce novel dosage forms in the field of drug development (Duan et al., 2014).

In SSE 3D printing, a semi-solid solution, gel, or paste is deposited layer-by-layer to create a 3D object according to a pre-determined computer-aided design (CAD), and upon curing or solidification, the final dosage form with desired size and shape is obtained. One main advantage of SSE 3D printing is that the printing can be performed at low temperatures, making it suitable for many different drugs, including thermosensitive ones. For instance, Germini et al. prepared an indomethacin nanocrystal-loaded fast-dissolving 3D-printed oral film. The drug crystals were prepared by conventional pearl milling (Germini and Peltonen, 2021). Schmidt et al. developed 3D-printed hydrophilic films loaded with triamcinolone acetonide in SBA-15-type mesoporous silica nanoparticles (MSNs). MSNs were synthesized and used in the nanoencapsulation of the drug (Schmidt et al., 2022). These studies explored combining nanotechnology and SSE 3D printing to print poorly water-soluble drugs.

In this study, we employed SSE 3D printing to prepare personalized films of nanoPRX produced by the robust, stable, and reproducible CESS® technique as a proof-of-concept study for other CESS®-produced nanoparticles. The main objective was to prepare a suitable printing ink that stabilized the nanoparticles to obtain the final dosage forms with the original polymorph of the nanoPRX. The prepared oral thin films exhibited accurate dosing with good mechanical properties with suitable dissolution profile. In addition, a stability study was conducted to ensure the stability of the particles in the prepared dosage forms for at least three months.

2. Materials

NanoPRX, provided by Nanoform Finland Plc. (Helsinki, Finland), was used as received. Three different polymers were studied for stabilizing the nanoPRX, hydroxypropyl cellulose (HPC), hydroxypropyl methylcellulose (HPMC), and a polyvinyl alcohol-polyethylene glycol graft copolymer (PEG-PVA). HPC (Klucel EXF) was kindly provided by Ashland (Schaffhausen, Switzerland) and PEG-PVA (Kollicoat Protect) by BASF SE (Ludwigshafen, Germany). Several HPMC grades from different producers with various methoxy and hydroxypropyl substitutions were investigated (specific details in (Table A.1). Tylopur (603, 605, and 606), Methocel (E5 Premium LV and K3 LV), and Benecel (K100 LV, K100 M, and K15 M) were kindly donated by SE Tylose GmbH & Co.KG (Wiesbaden, Germany), Dow Chemical Company (Bomlitz, Germany), and Ashland (Schaffhausen, Switzerland), respectively. Tween 80 was purchased from Sigma Aldrich (Steinheim, Germany). To prepare the aqueous polymer dispersions, three different film-forming polymers were investigated; HPMC (Tylopur® 605), HPC (Klucel™ EXF), and PEG-PVA (Kollicoat® Protect). Glycerol, purchased from Sigma Aldrich (St. Louis, MO, USA), was used as a plasticizer in the aqueous polymer dispersions. Purified water (MQ) (Milli-Q® water) and ethanol (EtOH) (Etax A 94 w-%, Altia Oyj, Rajamäki, Finland) were used as solvents. All water in this study was purified by a Millipore SA-67120 system from Millipore (Molsheim, France). To create a cross-section for SEM imaging, printed objects were frozen with liquid nitrogen (Oy Linde Gas Ab, Finland). Sodium phosphate monobasic (Sigma-Aldrich, Germany), sodium chloride (VWR International Oy, Finland), and sodium hydroxide (Merck, Germany) were used to prepare the phosphate media.

3. Methods

3.1. NanoPRX printing ink preparation

3.1.1. Preparations of nanoPRX suspension

Stabilization of nanoPRX in the aqueous suspension is required as evident in Fig. A.1 that shows the crystal growth of nanoPRX in an unstable solution. Therefore, different aqueous base solutions containing different polymers and amounts of them (Table A.2) combined with Tween 80 as a surfactant were prepared and investigated to determine the best way to stabilize the nanoPRX. The aim was to achieve the highest possible drug loading with a sufficient dynamic viscosity range that allows ink preparation. The aqueous base solutions were prepared by adding purified water, polymer, and surfactant in 100 mL borosilicate bottles by mixing them under continuous stirring for three hours. To evaluate the base solutions' performance, suspensions were prepared by mixing nanoPRX with the freshly made base solutions, stirring them at 800 rpm for 5 min, followed by 30 s of sweet (right on top of the ultrasound source) spot bath sonication, and then vortexing for a few seconds. The prepared suspensions were evaluated in different ways; visual inspection was performed to inspect for a potential color change, the particle size and polydispersity index (PDI) were determined with dynamic light scattering (DLS) measurement, transmission electron microscopy (TEM) analysis was conducted. The chosen aqueous base solutions contained 3.75% (w/w) HPMC (T-605) and 1% (w/w) Tween 80. NanoPRX was mixed with the base solution, so a final homogenous drug suspension was obtained containing 7.5% (w/w) nanoPRX. Hereafter referred to as the nanoPRX suspension.

3.1.1.1. Dynamic light scattering characterization. The particle size of a nanomaterial influences the surface area and impacts the dissolution rate (Hackley and Clogston, 2005). The particle size of the nanoPRX in the prepared suspensions was measured with DLS (Zetasizer Nano series, Malvern Instruments Ltd, Malvern, UK) and analyzed with Zetasizer software 7.11 (Malvern instruments limited). DLS is commonly used to measure the hydrodynamic diameter (Z-average) and PDI of nanoparticles in suspension (Clayton et al., 2016). The measurement was performed by illuminating the suspension of nanoparticles with a laser and analyzing the intensity fluctuations of the scattered light arising from the Brownian motion of the nanoparticles. The signal is analyzed using CUMULANTS-algorithm providing information about the hydrodynamic diameter and PDI. The hydrodynamic diameter includes the adsorbed or hydrated layer around the nanoparticle. The algorithm assumes a monodisperse particle size distribution, which is rarely the case,

and the PDI is used to estimate the error that polydispersity causes because of this assumption (Kaasalainen et al., 2017). The PDI value ranges from 0.0 to 1.0, for a perfectly homogenized sample to a highly polydisperse sample with multiple particle sizes. PDI values of < 0.2 are most commonly accepted in polymer-based nanoparticle materials. A sample is considered very monodisperse if the PDI < 0.05. On the contrary, if PDI > 0.7, it indicates that the material has a broad particle size distribution, and it is unsuitable to be analyzed with the DLS technique (Danaei et al., 2018; Sakho et al., 2017). In the current study, the prepared suspensions were diluted 10-fold with purified water and sonicated for 30 s, followed by vortexing for a few seconds prior to DLS measurement. Each sample was analyzed using 20 s of equilibrium time before measurement using ZEN0040 disposable cuvettes at 25 °C. Average and standard deviation were calculated (n=3), and the results guided the choice of the best suspension to move forward with. With higher polymer concentrations, the viscosity of medium changes even after 10-fold dilution leading to an increased Z-average. Hence, the dynamic viscosity of medium was estimated according to the equation provided by The Dow Chemical Company (2002).

3.1.1.2. Transmission electron microscopy. TEM is a technique in which a beam of electrons interacts with the sample by transmitting through the sample to produce an image of the nanoparticle (Wang et al., 2018). The morphology of nanoPRX in the chosen suspension was analyzed by TEM imaging (JEM-1400 Plus Electron Microscope, JEOL, Musashino, Akishma, Tokyo, Japan) in bright-field mode with an acceleration voltage of 80 kV. The sample was prepared by diluting the HPMC-based T-605 suspension of nanoPRX with purified water to a concentration of 0.01 wt% and sonicating for 1 min. Subsequently, 5 μL of the freshly prepared sample was transferred onto a carbon-coated copper grid (Ted Pella Inc., Redding, CA, USA) and incubated for 3 min at ambient temperature. The excess liquid was removed by blotting with filter paper before loading it into the microscope. The nanoPRX single particle size image obtained from TEM was manually measured using the open-source image analysis software (Fiji version 2.11.0, National Institutes of Health, Maryland, USA).

3.1.2. Preparation of aqueous polymer dispersions

The suspensions cannot directly be prepared to exhibit suitable rheological properties for SSE 3D printing. Therefore, three different polymers were investigated to prepare aqueous polymer dispersions to be mixed with the prepared suspensions to obtain suitable printing inks with nanoparticles embedded in the polymer matrix. The film-forming polymers investigated were Kollicoat Protect (KP, PVA-PEG), T-605, and Klucel EXF (K-EXF, HPC). The polymers were mixed in purified water and stirred on a magnetic stirrer for 24 h at room temperature until, preferably, smooth homogenous dispersions were obtained. The decision was made to move forward with the HPC and HPMC formulations, and the chosen final aqueous polymer dispersions were: 1) 25% (w/w) HPMC solution and 2) 25% (w/w) HPC solution with 4% (w/w) glycerol.

3.1.3. Preparation of printing inks

Characteristics of a good SSE 3D printing ink are easy preparation (preferably without heat), non-sticky, smooth, and even texture without lumps, and easy transferability into syringes. The printing ink should possess a high enough dynamic viscosity with shear-thinning properties to be printable but still prevent the ink from spreading out post-printing. Two printing inks were prepared by combining the chosen nanoPRX suspension with the two final aqueous polymer dispersions. The printing inks were formulated by mixing two parts of suspension with three parts of aqueous polymer dispersion (Table 1), to achieve 3% (w/w) drug loading in the final printing inks. Their corresponding drug-free placebo solutions were prepared in the same manner as drug-loaded printing inks without the addition of the nanoPRX suspension.

Table 1
Two drug-loaded printing inks were prepared by microfluidic mixing by combining the nanoPRX suspension with the two aqueous polymer dispersions in a 2:3 ratio.

PI	Suspension	Aqueous polymer dispersions
1	7.5% nanoPRX + 3.75% HPMC+ 1% Tween 80	25% HPMC
2	7.5% nanoPRX + 3.75% HPMC+ 1% Tween 80	25% HPC + 4% glycerol

PI: printing ink; nanoPRX: nanoformed piroxicam; T-605: Tylopur 605 (hydroxypropyl methylcellulose); HPMC: hydroxypropyl methylcellulose (T-605); HPC: hydroxypropyl cellulose. All % are in w/w ratios.

A microfluidic device (Pump 33 Dual Drive System (DDS) Syringe Pump, Harvard Apparatus, Massachusetts, US) was used to mix the suspension and aqueous polymer dispersions to obtain the final homogenized printing inks. The multi-purpose DDS syringe pump has two independent pumping channels controlled by a touchscreen interface. Four grams of suspension and six grams of aqueous polymer dispersion were placed in separate 10 mL syringes (BD Plastipak TM Luer-Lok, Becton Dickinson S.A., Madrid, Spain) and attached together by a Luer lock silicon tubing system. The filled syringes were clamped to separate pumps. The reciprocating operating condition was chosen, where both syringe channels move continuously in opposite directions at the same rate using the same syringe size and type. The test setup can be seen in (Fig. A.2). The pump speed is set for the characteristics of the solutions. The infuse and withdraw rates for both the drug-loaded and the placebo inks were set to 450 mL/h, the highest speed the system could withstand with the implemented set-up. The duration of the mixing is based on the set target value required to obtain a homogenized final printing solution. To mix and get the homogenous solution, the target was set to 400 mL and 300 mL, respectively, taking approximately 60 min to obtain homogenous drug-loaded inks and 45 min to obtain homogenous drug-free placebo solutions. The multi-purpose DDS syringe pump system was used to produce two different drug-loaded printing inks and corresponding placebo solutions.

3.1.4. Rheology

Rheology is used to determine the deformation and flow behavior of each material. In the current study, rheology was utilized to investigate the dynamic viscosity of printing inks 1 and 2 under the influence of shearing properties to determine their rheological properties before printing. The rheological properties of the printing solutions were analyzed with a HAAKE™ MARS™ 40 Advanced Modular Rheometer system (Version: 4.87.001, Thermo Scientific, Karlsruhe, Germany). The system was equipped with a 35 mm diameter rotor plate (P35/Ti) and a lower plate (TMP 35). The measuring gap was set to 0.5 mm, and the temperature was kept at 23 °C. The sample was pre-sheared for 30 s at a rate of 1 s^{-1}, followed by 60 s of equilibration. Afterward, the measurement was run with a shear rate ramp of 0.01–1000 s^{-1}, a running duration of 350 s, and an 8 s per data acquisition point. The HAAKE™ RheoWin job manager software recorded the measurements, and the obtained data were analyzed with the HAAKE™ RheoWin data manager (Version: 4.87.001, Thermo Scientific, Karlsruhe, Germany). Both printing inks were measured twice, and a third measurement was performed if any differences were observed between the two initial runs.

3.1.5. Computer-aided designs

Four circle designs were made using computer-aided design (CAD) software (Fusion 360, version 2020, Autodesk, San Rafael, CA, USA). The designs were saved as .stl files and sent to the slicer software (RepertierHost v1.6.1, Hot-World GmbH & Co. KG, Willich, Germany), where the print settings were set, and the g-code was generated. The films were designed to have sizes that would achieve therapeutic drug doses of up to 20 mg when printing with the 3% drug-loaded printing inks. The four different designs had an equal height of 0.5 mm and

diameters of 7.5, 10, 15, and 20 mm, equaling a surface area of approximately 44, 79, 177, and 314 mm^2, respectively. The prepared dosage forms will refer to films of sizes 7.5, 10, 15, and 20. Drug content measurements were performed on all four film sizes, and films of size 10 were used for additional analysis.

3.1.6. Semi-solid extrusion 3D printing

Printing inks 1 and 2 were printed with a Biobot (Allevi 2, Biobots Inc, Philadelphia, USA) 3D printer attached to an ultra-quiet and oil-free air compressor (California air tools, San Diego, California, US). The printing solutions were placed in new 10 mL BD Plastipak disposable syringes, attached with 21 G dispensing precision tips (Quantx precision dispense tips, Fisnar Europe, Scotland, UK), and printed on transparency sheets (Clear transparent X-10.0, Folex, Köln, Germany). The printed dosage forms were printed with a layer height of 0.5 mm, using a rectilinear fill pattern with a 45° angle, and the infill density and infill overlap was set to 80%. To achieve therapeutic doses, the printing pressure had to be adjusted to fit the different viscosities of the two prepared printing inks. Printing ink 1 was printed at a set pressure of 117 kPa (17 PSI), and printing ink 2 at 193 kPa (28 PSI). Both inks were printed with a printing speed of 8 mm/s.

3.1.7. Drying processes

The CESS®-produced nanoPRX has a crystal structure of the anhydrous form I, which provides a small particle size that is stable in dry form. The particle's stability in an aqueous solution may be challenged by Ostwald ripening and recrystallization to PRX monohydrate. It can take up to 48 h for the printed dosage form to fully dry under ambient conditions, potentially causing crystallization (Aminuddin et al., 2011). To prevent this, as well as to understand the impact of drying the dosage form, two different drying processes were investigated. The first drying process was drying at ambient conditions for 48 h at 22.2 ± 0.1 °C and 29.6 ± 2.5% relative humidity (RH). The second investigated drying process was freeze-drying, which was carried out by first placing the freshly printed samples in an ultra-low temperature freezer set to -80 °C (SANYO Electric Biomedical Co., Ltd, Nakamura-ku, Japan) for 15 min, followed by drying for 15 h utilizing the Heto CT 60 e (Allerod, Denmark) system, equipped with oil mist filter EMF10 vacuum (Edwards high vacuum international, West Sussex, England). All samples were visually analyzed, and their flexibility was determined. The samples were stored at ambient conditions before further analysis.

3.2. Characterization of the SSE 3D-printed films

The printed dosage forms produced from printing inks 1 and 2 were visually analyzed. The mechanical strength, moisture content, disintegration time, *in vitro* dissolution, and drug content were determined. Mechanical strength and moisture content were performed on both room temperature-dried (RTD) and freeze-dried (FD) samples and their corresponding placebos. Disintegration time and *in vitro* dissolution profiles were determined for the drug-loaded RTD and FD samples. Drug content determination was only performed on the drug-loaded RTD samples, and the corresponding placebos were used as references.

3.2.1. Physical appearance

The appearance of the printed dosage forms was visually evaluated and photographed. The thickness of each printed film was measured with a caliper (Absolute Digimatic, Mitutoyo, CD-6 "CX, Kawasaki, Japan) at three points of the films. The weight of the films was determined using an analytical balance (Radwag Wagi Elektroniczne, Radom, Poland), and average and standard deviations was calculated.

3.2.2. Scanning electron microscopy

Scanning electron microscopy (SEM) uses an electron beam to produce images on a scanned surface of a solid sample with nanometer-scale resolution. The field emission SEM Zeiss Sigma 300 VP (Carl Zeiss Microscopy Deutschland GmbH, Germany) was used to capture the images on the printed drug-loaded and drug-free placebo samples. The samples were frozen using liquid nitrogen, cracked, and transferred to a 90° aluminum SEM sample holder equipped with double-sided carbon tape. Subsequently, the samples were coated with a 5 nm thick layer of platinum to render the material conductive prior to imaging.

3.2.3. Mechanical strength

For adequate handleability when manufacturing, packing, and administering a dosage form, the dosage form must exhibit sufficient mechanical strength. In the current study, a puncture test was performed as per Sjöholm et al. (2020), except that a cylindrical probe (P/5, TA.XT. Plus Texture Analyser, Godalming, UK) was used instead of the ball probe. Each measurement was performed five times under ambient conditions. The ambient conditions were 22.0 ± 0.2 °C and 30.7 ± 0.9% RH for all samples except for the films prepared from the corresponding placebo solution to printing ink 2, which was measured on another day with conditions of 22.3 ± 0.1 °C and 44.7 ± 0.1% RH. Averages and standard deviations were calculated. In addition, statistical analysis was carried out using statistical software (GraphPad Prism version 9.5.1 Crack Build 733). The column analyzes unpaired t-test was employed to find the statistical significance. A different comparison test was conducted by comparing the printing ink 1 and 2, drug-loaded, and their corresponding placebo films of force (N) and distance (mm). The two-tailed P value was obtained at a 95% confidence level.

3.2.4. Moisture content

Determining the moisture content in the dosage forms is important, as a too high or too low moisture content may affect the stability of the dosage forms. Some water content might be necessary as water acts as a plasticizer and may give polymeric films more flexibility than completely dry films that are often brittle, reducing their handleability. Too high water content may yield sticky films and increase the possibility of microbial growth (Lir et al., 2007). The moisture content of the prepared dosage forms was determined in accordance with Sjöholm et al. (2020) by placing approximately 0.5 g of sample on the aluminum pan by measuring the change in weight while heating the sample to 120 °C. The weight loss of evaporated moisture mass % was recorded, and each measurement was made in triplicate under the same ambient conditions as stated in Section 3.2.3.

3.2.5. Drug content

In the preparation of personalized dosage forms, precise drug content is an important attribute. To analyze the drug content, the drug must be fully dissolved. Hence a 1:1 (v/v) MQ:EtOH solvent mixture was chosen as media. Accurately weighed dosage forms printed with printing inks 1 and 2 and dried at ambient conditions (n=5) were placed in 100 mL borosilicate bottles containing 50 mL of media. The bottles were shaken on an orbital shaker (Multi-shaker PSU 20, Biosan, Riga, Latvia) for three hours until completely dissolved. Samples were withdrawn, and appropriately diluted, and the concentration was measured with UV-Vis spectrophotometry (UV-6300PC Double Beam Spectrophotometer, VWR International BVBA, Leuven, Belgium) at 357 nm. The average drug content and standard deviations (n=5) were calculated against a predetermined calibration curve using corresponding placebos as blank measurements to omit possible interference from the excipients.

3.2.6. Disintegration of films

The disintegration time of drug-loaded films is an attribute that determines the character of the dosage form. According to the European Pharmacopeia, different dosage forms should disintegrate within given time frames (The Dow Chemical Company 2022). In the present study, the disintegration time of the printed films was determined in the same manner as Sjöholm et al. (Sjöholm et al., 2020). The test was performed on size 10 RTD and FD films printed with printing ink 1 and 2 (n=6). Average and standard deviation were calculated.

3.2.7. In vitro dissolution

The dissolution study was carried out using the USP type 1 apparatus Erweka (Langen, Germany), along with the in-situ fiber optic concentration monitoring system Pion Rainbow R6 UV probe (East Sussex, England) with a path length of 2 mm. The second derivative spectrum was used for the analysis to minimize the effect of non-dissolved nanoparticles, and the area under the curve at the wavelength range of 300–320 nm was used to quantify the adsorption. The test was performed on the size 10 pre-weighed nanoPRX-loaded printed films and placed in the dissolution vessels containing 900 mL phosphate buffer pH 6.5. The dissolution bath was set to 37±0.5 °C, and the baskets were set to rotate at 100 rpm. The dissolution study was carried out for 120 min (n=3). The concentration data were normalized based on the theoretical loading of piroxicam in printed objects. The size of all the printed objects was the same, but due to the additive glycerol in printing ink 2, the loading degree of the inks slightly differed.

3.3. Solid-state analysis

PRX has three different polymorphic forms: α, β, and monohydrate pseudopolymorph (Maruyama and Ooshima, 2001; Redenti et al., 1999). Solid-state analysis was performed on pure nanoPRX, PRX monohydrate, drug-loaded films, and corresponding placebos. PRX monohydrate was used as a reference to investigate polymorphic changes in the prepared films. Therefore, PRX monohydrate was prepared by dissolving nanoPRX in water, upon which a bright, yellow-colored suspension was obtained that was subsequently dried to attain PRX monohydrate crystals for analysis. Several techniques were utilized for the solid-state analysis. Attenuated total reflectance-Fourier transform infrared spectroscopy (ATR-FTIR) was used to investigate the structure and properties of the materials. Raman spectroscopy was utilized to analyze the polymorphic forms of nanoPRX, and the structure of the crystalline material was analyzed by X-ray powder diffraction (XRPD).

3.3.1. Attenuated total reflectance Fourier transform infrared spectroscopy

The structure and properties of pure nanoPRX, drug-loaded dosage forms, and their corresponding placebos were analyzed using the same set-up as in the study by Sjöholm et al. (2020), utilizing ATR-FTIR spectroscopy (UATR Spectrum Two, PerkinElmer Inc., Buckinghamshire, UK). The measurement was carried out twice on each sample. In addition, a third measurement was carried out in case differences were observed between the first two measurements.

3.3.2. Raman spectroscopy

The solid-state forms of nanoPRX were investigated by Raman spectroscopy (Nicolet iS50 Raman by Thermo Fisher Scientific (Waltham, MA, USA) equipped with a 1064 nm diode laser and an InGaAs detector). It also gives information about the chemical structure, phase, crystallinity, and molecular interactions of the materials. Pure nanoPRX, PRX monohydrate drug-loaded dosage forms, and corresponding placebos were measured in the same manner as in our previous study by Sjöholm et al. (2022).

3.3.3. X-ray powder diffraction

XRPD is a powerful, non-destructive, rapid technique used to identify and characterize crystalline materials and provide information about unit cell dimensions. The nanoPRX containing SSE 3D-printed films were evaluated using Malvern PANalytical Empyrean X-ray diffractometer (Malvern Panalytical Ltd, Malvern, UK), equipped with a Cu Kα (1.54 Å) source, MultiCore optics, and a solid-state PIXcel3D detector. The printed dosage forms were attached to aluminum sample holders using double-sided Kapton tape. The samples were measured in the reflection geometry in a spinning stage with a 5-40 (2θ) measurement range. The step size and time per step values were varied depending on the counts per second obtained. Typical measurement times per sample ranged from 30 min to 3 h.

3.4. Stability study

A one-month stability study was performed to investigate the nanoPRX stability in the prepared RTD and FD dosage forms and to explore the presence of interactions and polymorphic changes. Films of size 10 were placed in Petri dishes to be stored in ambient conditions and analyzed one month after printing. The solid-state was evaluated by ATR-FTIR and Raman spectroscopy in accordance with Sections 3.3.1 and 3.3.2, respectively. In addition to the one-month stability study, the stability of the nanoPRX in the prepared dosage forms stored for three months at room temperature and 75% RH was investigated by XRPD per Section 3.3.3.

4. Results and discussion

4.1. NanoPRX printing ink preparation

4.1.1. Preparation of nanoPRX suspensions

The main goal when preparing the nanoPRX suspensions was to disperse and stabilize the nanoPRX particles in an aqueous base solution. PRX exhibits a distinct color change from white to bright yellow when recrystallizing to the monohydrate form (Sheth et al., 2005), and this facilitated the formulation preparation. Initially, nanoPRX was mixed with an aqueous base solution containing only Tween 80, but the suspension quickly obtained a bright yellow color indicating that Tween 80 alone is not able to stabilize the nanoPRX in the suspension. Hence, several known stabilizing grades of HPMC were investigated to render a base solution able to stabilize the nanoPRX (Fig. A.1). Multiple base solutions of different polymers in different amounts (Table A.2) and in combination with Tween 80 as a stabilizer was prepared. Subsequently, different amounts of nanoPRX were mixed with the prepared base solutions. The objective was to obtain white, milky, high-drug-loaded suspensions. The selections steps to identify the most suitable stabilizing polymers are visualized in a flow chart (Fig. 1). The suspensions containing Methocel K3 LV, Benecel K100 M, HPC, and KP (suspensions 5, 6, 9, and 10) obtained a bright yellow color when stored overnight and were excluded from further studies. We can only speculate on the reason behind the insufficient stabilization of nanoPRX. It is known that a high amount of hydrophobic substitution is essential in stabilizing the drug in a suspension. Furthermore, the molecular weight affects the crystallization inhibition effect, where a higher molecular weight shows a higher inhibition to a certain degree (Yang et al., 2016). HPC and KP do not exhibit methoxy and hydroxypropyl substitution and are unable to stabilize the hydrophobic nanoPRX. Methocel K3 LV and Benecel K100 M contain the methoxy and hydroxypropyl groups, but due to the very low molecular weight of Methocel K3 LV (<10,000) and the very high molecular weight of Benecel K100 LV (1,000,000), the polymers were not good stabilizers. Suspensions containing Tylopur 603, 605, and 606, Methocel E5 Premium LV, Benecel K100 LV, and K15 M (suspensions 1-4, 7, and 8) did not turn yellow and were hence further investigated by DLS. HPMC-based polymers can be divided into type E and type K based on their substitution grade; the decision was made to choose one of each type for further investigations. HPMC type E polymers are considered a more effective crystallization inhibitor due to the ratio between the hydrophobic and hydrophilic substitution compared to type K HPMC polymers (Yang et al., 2016). T-605, a type E polymer, showed superior DLS results by exhibiting the lowest Z-average value and was chosen for further investigation (Table A.2) of the type K polymers, Benecel K100 LV showed adequate DLS results. However, it performed the best of its group and was hence chosen for further investigation as a point of reference. To achieve a 3% drug-loading in the final ink formulation, the drug loading in the suspension had to be increased. To sufficiently stabilize the increased amount of drug in the suspension, the polymer, and the plasticizer amounts were likewise

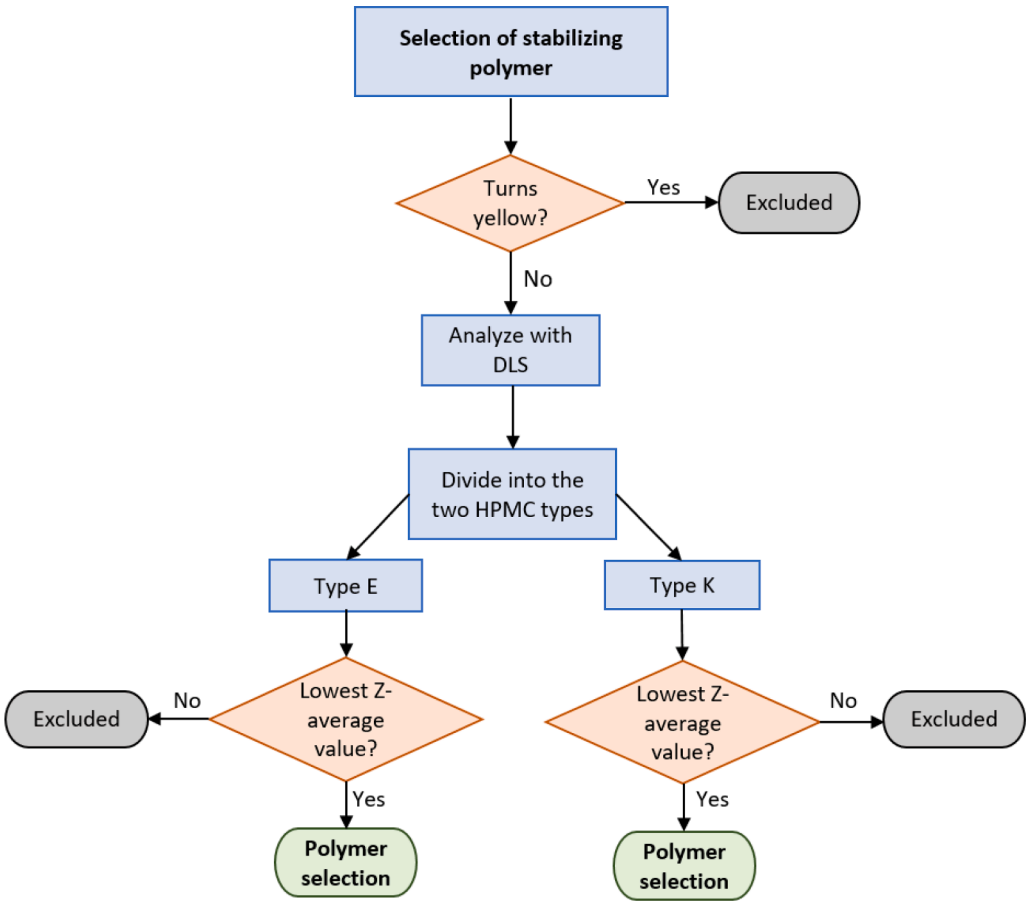

Fig. 1. Selection steps for finding the most appropriate polymer to stabilize the nanoPRX in the suspension.

increased. Increasing the amount of Tween 80 facilitated the stabilization of the particles. Suspensions with nanoPRX-loading of 5%, 7.5%, and 10% (w/w) were successfully prepared with T-605 and B-K100 LV, exhibiting low, medium, and high viscosity, respectively. The suspension with the 10% loading had unpractically high viscosity so the suspension containing 7.5% nanoPRX, was chosen for further studies. As expected, the type E HPMC polymer, i.e., T-605, exhibited better performance based on the DLS results. Therefore, the suspension containing 3.75% T-605 and 1% Tween 80 was prepared with the highest possible drug loading of 7.5%.

4.1.1.1. Dynamic light scattering characterization. The Z-average of nanoparticles in the prepared suspensions were determined with DLS. The Z-average diameter increased with increasing nanoPRX concentration in the suspension (Table A.2). The final suspension containing T-

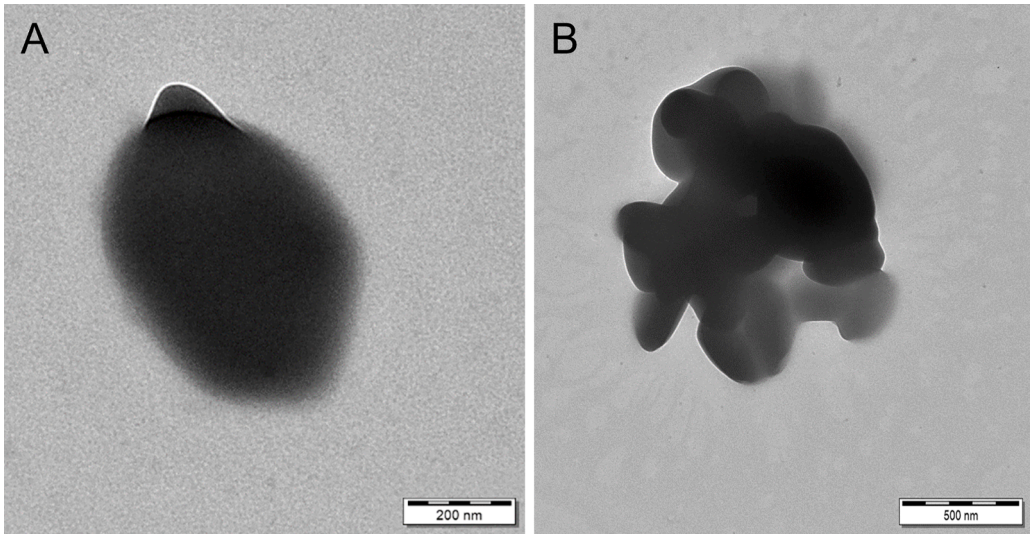

Fig. 2. Transmission electron microscopy images of nanoPRX particles in a hydroxypropyl methylcellulose (HPMC)-based suspension (HPMC Tylopur 605). A) A single particle at a magnification of 20 000 x and B) agglomerated particles at a magnification of 12 000 x.

605 as stabilizing polymer exhibited a Z-average diameter of 388 ± 16 nm and a PDI value of 0.168 ± 0.095 (Table A.2). This corresponds to the previously acquired SEM micrographs of dry nanoPRX (Fig. A.3). The obtained PDI values for all prepared solutions, including the final suspension, ranged from 0.1 and 0.2, indicating that all prepared suspensions were well dispersed (Danaei et al., 2018; Kompella, 1999; Möschwitzer et al., 2004).

4.1.1.2. Transmission electron microscopy. The size of the nanoPRX particles in the prepared suspension was measured with TEM. The appearance of a single particle (A) and the agglomerated particles (B) can be seen in Fig. 2. The particle size was measured with Fiji software to be around 375 nm, which confirms the DLS findings in the current study, as well as in a previous study (Kaasalainen et al., 2017). Stabilizers play a significant role in preventing the nanoparticles from aggregating and agglomerating during preparation. However, agglomeration is hard to avoid, and some were found in the prepared suspension. An increased amount of Tween 80 could potentially have prevented the agglomeration of the nanoPRX by forming a steric barrier around the particles (Esfandi et al., 2014).

4.1.2. Preparation of aqueous polymer dispersions

To obtain a homogenous nanoPRX printing ink with suitable viscosity without compromising the stability of the nanoPRX, the aqueous polymer dispersions were prepared separately, and were subsequently combined with the prepared suspension. The chosen polymers were Kollicoat Protect (PEG-PVA), Klucel EXF (HPC), and Tylopur 605 (HPMC); 25% (w/w) aqueous polymer dispersions were prepared with all three polymers, with and without glycerol under continuous slow mixing on a magnetic stirrer for up to 24 h.

PEG-PVA was unsuitable for the preparation of the aqueous polymer dispersion as it requires high heat (70 °C) to dissolve, and the final dispersions were neither smooth nor even; instead, the dispersion featured large lumps. No further studies were conducted with PEG-PVA. A clear, smooth dispersion was obtained when preparing the aqueous HPC dispersion with glycerol, while the dispersion without glycerol became foamy and contained bubbles and lumps. The aqueous HPMC dispersion with glycerol required extensive time to dissolve, and the obtained dispersion was foamy and featured bubbles and lumps, whereas the aqueous HPMC dispersion without glycerol rendered a smooth and clear dispersion. The presence of lumps in a printing ink is unacceptable as it causes clogging and uneven printing, consequently leading to inaccurate and unreliable drug dosing. Therefore, two aqueous smooth and clear aqueous polymer dispersions were chosen, the first one consisting of 25% (w/w) HPMC and the second one of 25% (w/w) HPC and 4% (w/w) glycerol.

4.1.3. Preparation of printing inks

Two printing inks were prepared by combining the prepared nanoPRX-containing suspension with the two prepared aqueous polymer dispersions by mixing two parts of the suspension with three parts of the aqueous polymer dispersion to obtain a 3% (w/w) drug loading in the final printing inks. Preparing a homogenous printing ink was challenging. Initially, mixing the two solutions was attempted by agitation by a magnetic stirrer and manual mixing from one syringe to another. Both failed to produce homogenous solutions and in addition, the latter was laborious. A more automated approach was desired, and thus, a microfluidic device was investigated and utilized. The homogeneity of the produced drug-loaded and drug-free placebo printing solutions was visually determined. The HPMC-based printing ink 1 was easier to mix with a microfluidic pump due to its lower viscosity. Some practical difficulties were experienced in preparing the HPC-based printing ink 2 due to its higher viscosity. Both drug-loaded printing inks had a suitable viscosity for SSE 3D printing and exhibited a pure white color after the addition of nanoPRX. The drug-free placebo solutions were smooth and clear, but without the drug, they exhibited a lower viscosity than the drug-loaded printing inks and were unsuitable for printing and were hence manually extruded for the needed analysis.

4.1.4. Rheology

The rheological behavior of the final drug-loaded printing inks and their corresponding drug-free placebo solutions were analyzed to estimate their printability. Viscosities (Pas) as a function of shear rate (1/s) were plotted in Fig. 3. Printing ink 2 contains HPC, which has four-times higher molecular weight than the HPMC in printing ink 1, resulting in a higher dynamic viscosity compared to the HPMC-based printing ink. The drug-loaded formulations exhibited a higher dynamic viscosity than the placebo formulations due to the intermolecular interactions between excipients and nanoparticles (with high surface area), as well as the increased solid content. This has been previously reported (Sjöholm et al., 2020; Reis and Derby, 2003; Nallan et al., 2014). The rheological results confirm the viscous properties observed during the preparation and printing of the drug-loaded inks and their corresponding drug-free placebo solutions. All printing inks showed shear-thinning behavior, which is necessary for SSE 3D printing.

4.1.5. Semi-solid extrusion 3D printing

NanoPRX containing printings ink 1 and 2 were successfully printed with the Biobot SSE 3D printer, and different-sized drug-loaded films were obtained. The four different designs were printed with an escalating size according to their area (mm^2), with a significant correlation between the designed size and obtained drug amount. The viscosity measurements indicate that printing ink 1 exhibited a lower viscosity than printing ink 2, which also accounts for the differences in the required printing pressure to obtain therapeutic doses up to 20 mg.

4.1.6. Drying processes

The nanoPRX-containing printed films of printing ink 1 and 2 took 24 h and 48 h, respectively, to completely dry under ambient conditions. A slight color change from white to pale yellow was observed in the dried films. This subtle color change raised concerns regarding the stability of nanoPRX in the aqueous base solution for prolonged times since PRX might recrystallize in the presence of water (Bordner et al., 1984). Hence freeze-drying was explored to decrease the drying time and to potentially prevent possible recrystallization of the nanosized drug. The films took 15 h to dry by freeze-drying and resulted in white-colored, porous films. In further studies by ATR-FTIR (0) and Raman analysis (0), it was found that the color change in the films dried at room temperature was unrelated to the crystallization of PRX to monohydrate formation. Despite this finding, both RTD and FD films were further investigated.

4.2. Characterization of 3D printed films

4.2.1. Physical appearance

White-colored nanoPRX-containing films with a slight yellow hue of different sizes were obtained by Biobot SSE 3D printing. The RTD and FD drug-loaded films of escalating area printed with printing ink 1 and 2 shown in Fig. 4. The weight of the dried films ranged from 30 mg to 150 mg, with statistically significant correlation to the designed size, $R^2 =$ 0.9981 and 0.9988 for printing ink 1 and 2, respectively. Both inks gave similar escalating thicknesses from 0.2 to 0.4 mm, increasing with size due to the surface tension. The RTD films were smooth, while the FD films featured a rough surface due to the porous structure. Both RTD and FD films obtained from printing ink 1 became brittle upon drying, while the films obtained from printing ink 2 were flexible. Brittle films are hard to handle issues, and hence flexible films are preferred. However, the films obtained with printing ink 1 were easier to remove from the sheet after drying compared to films obtained from printing ink 2.

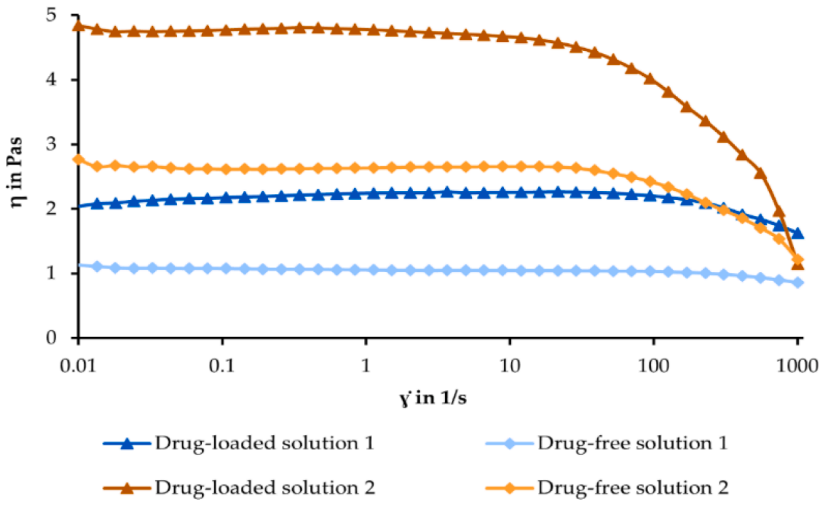

Fig. 3. Flow curves of printing ink (PI) 1 and 2 and their corresponding drug-free placebo solutions. PI 1 is visualized in blue, and PI 2 is visualized in orange.

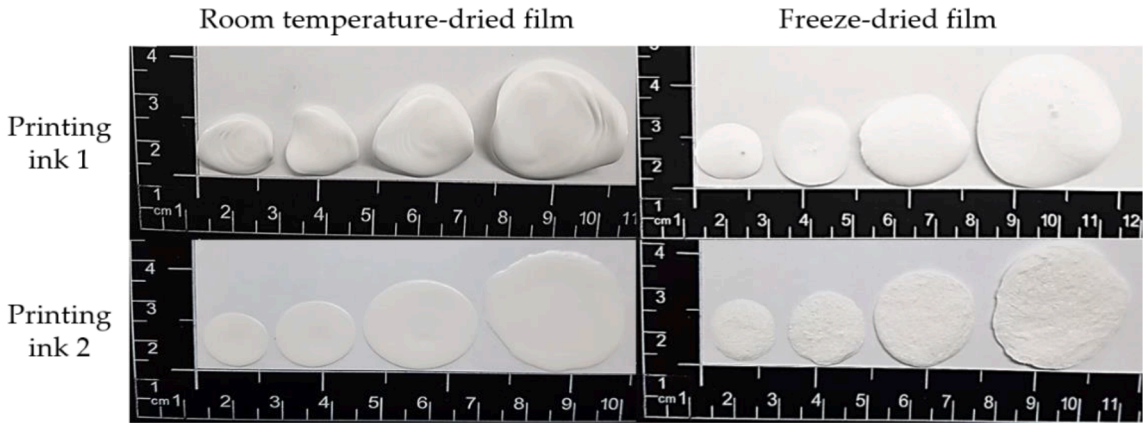

Fig. 4. Images of the room temperature-dried (RTD) and freeze-dried (FD) printed nanoPRX-containing films of different sizes printed with printing ink (PI) 1 and 2 containing 3% (w/w) nanoPRX.

4.2.2. *Scanning electron microscopy*

Cross-sectional SEM images of the RTD and FD drug-loaded films and their corresponding drug-free placebo films, printed with printing ink 1 and 2 are shown in Fig. 5. The nanoPRX particles were visible in the focused area of the drug-loaded films printed with printing ink 1. In contrast, as expected, no particles are visible in the drug-free placebo films. The particles observed in the drug-loaded film indicate the presence of nanoPRX and that the particles are not agglomerated in the films but distributed as individual primary particles (Fig. A.3). When comparing drug-loaded films of printing ink 1 and 2, the particles are visible in the films of printing ink 1, while in the drug-loaded films of printing ink 2 no particles are visible. Printing ink 2 consists of HPC and glycerol, which have film-forming properties leading to a smooth surface covering the nanoparticles (Hiremath et al., 2018). A very high porosity of FD HPMC-based film was observed, explaining the significant difference in dried film thickness (Fig. A.4).

4.2.3. *Mechanical strength*

Mechanical properties of the films were investigated by performing a puncture test to explore their durability and handleability. The test was performed on size 10 RTD and FD films obtained from printing ink 1 and 2 and their corresponding placebos. The puncture test measures the force it takes to burst the film expressed as maximum force (N), whereas the travel distance (mm) indicates the film's flexibility. The results of the strength and flexibility of the printed films are summarized in Table 2. The results of the unpaired t-test statistical analysis on different variables of RTD and FD films of printing ink 1 and 2 are summarized in Table 3. Films printed with printing ink 1 were generally stronger but less flexible than those printed with printing ink 2. The obtained statistical data indicates a statistical significance between the films of printing ink 1 and 2. Drug-loaded films commonly exhibit lower strength and flexibility than drug-free placebo films due to the presence of particles in the matrix (Öblom et al., 2019; Sjöholm and Sandler, 2019). For printing ink 2, the drug-loaded films exhibited statistically higher strength ($p<0.0001$) but lower flexibility than their corresponding drug-free placebo films. The films printed with the corresponding drug-free placebo solution to printing ink 2 were measured on a different day when the relative humidity was higher, which may explain the results. HPC and HPMC are both hygroscopic polymers (Mohammed et al., 2012; Panraksa et al., 2020), affecting their physical and possibly chemical properties. It was expected that the FD films would exhibit both lower strength and flexibility due to their porous structure. As expected, the strength of the FD films compared to RTD films was lower, with a statistical significance of $p\leq0.001$, but the flexibility was maintained even after freeze-drying.

4.2.4. *Moisture content*

The presence of moisture in the film affects the brittleness and friability behavior of the films, and an ideal oral film should have a moisture content below 5% (Nair et al., 2013). Excess moisture content can

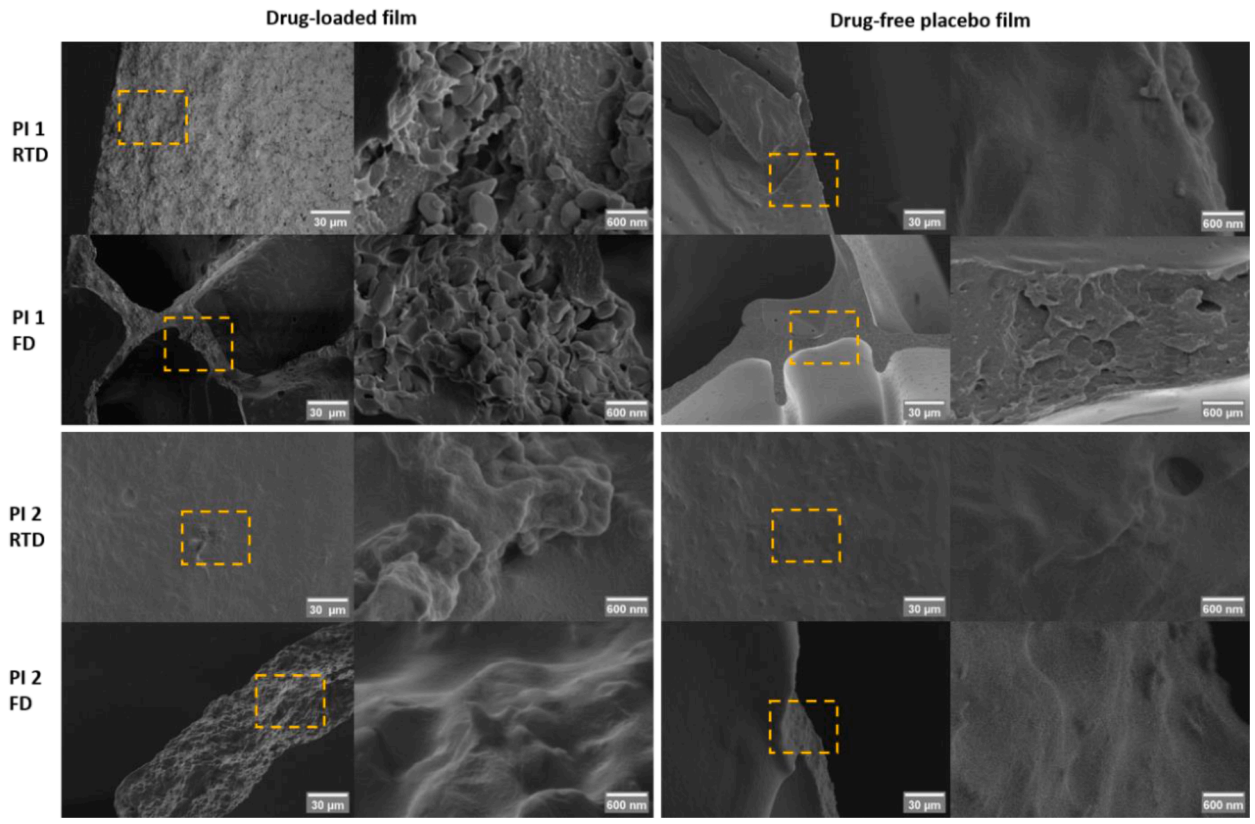

Fig. 5. Scanning electron microscopy images of printed nanoPRX films of both room temperature-dried (RTD) and freeze-dried (FD) films obtained with magnification of 500 x (left side figure with a yellow box) and 25 000 x (right side figure, magnification from the yellow box). A) Represents a drug-loaded and drug-free placebo film printed with printing ink (PI) 1, and B) represents a drug-loaded and drug-free placebo film printed with PI 2.

Table 2
Mechanical strength was measured by a puncture test performed on dried films printed with printing ink (PI) 1 and 2 and their corresponding drug-free placebos films, all dried at either room temperature or freeze-dried. Average and standard deviation (n=5).

Sample			Thickness (mm)	Force (N)	Distance (mm)	RH (%)	Temp.(℃)
PI 1	**Drug-loaded**	**RTD**	0.50 ± 0.12	25.37 ± 5.15	0.75 ± 0.06	30.1 ± 0.7	22.2 ± 0.1
		FD	1.51 ± 0.09	12.76 ± 1.82	0.75 ± 0.07		
	Drug-free	**RTD**	0.32 ± 0.05	65.09 ± 18.10	1.81 ± 0.30	30.1 ± 0.7	22.2 ± 0.1
		FD	1.45 ± 0.09	16.70 ± 1.95	1.13 ± 0.20		
PI 2	**Drug-loaded**	**RTD**	0.27 ± 0.01	13.74 ± 1.31	1.91 ± 0.09	31.2 ± 0.2	21.9 ± 0.0
		FD	0.41 ± 0.04	7.44 ± 1.85	1.76 ± 0.11		
	Drug-free	**RTD**	0.22 ± 0.02	4.19 ± 0.44	2.30 ± 0.18	44.7 ± 0.1	22.3 ± 0.1
		FD	0.35 ± 0.07	3.19 ± 0.94	2.31 ± 0.17		

PI: printing ink, RTD: room temperature-dried, FD: freeze-dried, RH: relative humidity, Temp.: temperature.

Table 3
A statistical analysis of unpaired t-test was carried out on the drug-loaded and their corresponding drug-free placebo films of printing ink 1 and 2.

Comparative unpaired t-tests	Variables	Analyzed data	*P* value	P value summary	Significantly different (P<0.05)?
DL vs. P	Strength	PI 1	0.0298	*	Yes
DL vs. P	Strength	PI 2	<0.0001	****	Yes
DL vs. P	Flexibility	PI 1	<0.0001	****	Yes
DL vs. P	Flexibility	PI 2	<0.0001	****	Yes
RTD vs. FD	Strength	PI 1 DL	0.0009	***	Yes
RTD vs. FD	Strength	PI 2 DL	0.0003	***	Yes
RTD vs. FD	Flexibility	PI 1 DL	0.9846	Ns	No
RTD vs. FD	Flexibility	PI 2 DL	0.0532	Ns	No

PI: printing ink, RTD: room temperature-dried, FD: freeze-dried, DL: drug-loaded, P: placebo. ****: $p \leq 0.0001$, ***: $p \leq 0.001$, **: $p \leq 0.01$, *: $p \leq 0.05$, non-significant (ns): $p > 0.05$.

potentially affect the film and make it prone to microbial growth (Pechová et al., 2018). A moisture analyzer was utilized to determine the moisture content of the prepared films of printing ink 1 and 2, RTD and FD, and their respective placebos films. The results are shown in Table 4. All drug-loaded films had a moisture content below 5%. The drug-free placebo films exhibited a slightly higher moisture content than their

Table 4
Moisture content (MC) of printed films of printing ink (PI) 1 and 2 and their placebos of films dried either at room temperature or in a freeze drier. Average and standard deviation (n=3).

Drying method	Printing ink 1		Printing ink 2	
	Drug-loaded (%MC)	Placebo (% MC)	Drug-loaded (%MC)	Placebo (% MC)
Dried at room temperature	3.8 ± 0.3	4.4 ± 0.1	2.1 ± 0.3	3.5 ± 0.6
Freeze-dried	3.1 ± 0.1	4.7 ± 0.3	3.6 ± 0.2	5.6 ± 0.4

corresponding drug-loaded films. No significant difference could be observed between the two drying procedures.

4.2.5. Drug content

The measured drug content in the printed films of different size obtained from printing ink 1 and 2, dried at ambient conditions, are presented in Table 5. Similar content results were found for both printing inks, with therapeutic doses ranging from below 5 mg to above 20 mg. Significant correlations between the designed size and the measured drug amount were achieved. The obtained R^2 values were 0.9965 and 0.9946 for printing ink 1 and printing ink 2, respectively. This demonstrates that the microfluidic mixing technique was successfully employed to produce homogenized printing inks and that SSE 3D printing is a suitable technique for producing personalized dosage forms by simply adjusting the design.

4.2.6. Disintegration of films

The disintegration time for all the prepared drug-loaded films was investigated. Due to the porous structure of the freeze-dried films, the assumption was that a more rapid disintegration would be observed compared to the films dried at ambient conditions. However, it was found that films printed with printing ink 1 and dried at different conditions had similar disintegration times of less than 10 min despite the different morphology. The films printed with printing ink 2 had a longer disintegration time when dried at room temperature, while the porous structure of the freeze-dried films expedited the disintegration, cutting the disintegration time in half. The disintegration time for the film obtained from printing ink 1 and 2, dried at different temperatures, can be seen in Table 6. The European Pharmacopoeia does not have a set disintegration limit for oral films (Tablets 2018). The average disintegration time of all the films was equal to or 15 min, corresponding to the time set for uncoated tablets. Adding a disintegrant to the formulation could expedite the disintegration if an orodispersible dosage form were desired.

4.2.7. In vitro dissolution

The dissolution rate of nanoPRX was analyzed in the different dosage forms and are presented in Fig. 5. Previously a dissolution study was carried out comparing micron-sized PRX and nanoPRX (Lakio and Sandler, 2020) and nanoPRX exhibited a faster dissolution rate

Table 5
Drug content of semi-solid extrusion 3D printed nanoPRX-containing films of printing ink (PI) 1 and 2. Average and standard deviation (n=3).

Film Size (Ø mm)	Area (mm^2)	Printing ink 1 Dry Mass (mg)	Printing ink 1 Drug Content (mg)	Printing ink 2 Dry Mass (mg)	Printing ink 2 Drug Content (mg)
7.5	44.18	28.64	4.78 ± 0.17	29.9	4.40 ± 0.24
10	78.54	46.2	6.90 ± 0.48	50.2	6.36 ± 0.26
15	176.71	81.64	12.26 ± 0.47	92.78	13.62 ± 0.75
20	314.16	141.54	21.90 ± 1.73	155.78	21.01 ± 0.89

Table 6
Disintegration of drug-loaded printed films of printing ink 1 and 2 dried either at room temperature or in a freeze-drier. Average and standard deviation rounded to full minutes (n=6).

Drying method	Printing ink 1 (min)	Printing ink 2 (min)
Dried at room temperature	8 ± 0	15 ± 2
Freeze-dried	9 ± 1	8 ± 2

compared to micron-sized PRX. In the current study, the dissolution profiles of the RTD and FD films of printing ink 1 and 2 are plotted as normalized concentration vs. time and visualized in Fig. 6. Films printed with printing ink 1 showed almost complete drug release within 30 min, 94% and 96% drug release for RTD and FD films, respectively. The drug release was slower for films of printing ink 2. However, FD films of printing ink 2 had a similar onset of action as the RTD and FD films of printing ink 1; but RTD films of printing ink 2 exhibited a delayed release. HPMC and HPC are hydrophilic cellulosic polymers, where HPMC is substituted with methoxy and hydroxypropyl groups, while HPC is substituted with only hydroxypropyl groups (Viridén et al., 2009). Hydrophilicity affects the drug release and swelling performance of matrix tablets (Alderman, 1984). HPC polymers are non-ionic, releasing the drug by a mechanism of swelling and erosion (Mohammed et al., 2012). The viscosity of the polymers also affects drug release. In our study, the HPMC-based polymer dynamic viscosity is lower than the HPC-based polymer, which was observed in the rheological results of the polymer-based solutions. Therefore, the lower molecular weight and viscosity might expedite the drug release in printing ink 1 compared to printing ink 2 that consists of HPC. The dissolution rate acceptance criteria by the European pharmacopoeia for an immediate release dosage form, is that more than 75% or 80% of the drug must be released within 15 min or 30 min, respectively (Tablets 2023). The criteria are met for three of the four tested dosage forms.

4.3. Solid-state analysis

The current study investigated these different polymorphic forms by different polymorphic characterization techniques. Analysis was performed on the pure nanoPRX and on the printed films of the two different printing inks by ATR-FTIR, XRPD, and Raman spectroscopy.

4.3.1. Attenuated total reflectance Fourier transform infrared spectroscopy

The ATR-FTIR was used to characterize different polymorphic forms in the pure nanoPRX, PRX monohydrate, and RTD and FD printed films from printing ink 1 and 2. The obtained ATR-FTIR spectra from 1700 cm^{-1} to 600 cm^{-1} are presented in Fig. 7. The literature states that the α and β forms have similar intramolecular structures but different intermolecular and hydrogen bond interactions (Redenti et al., 1999). Characteristic peaks of the α form appear at 1543 cm^{-1} and 1532 cm^{-1}. The latter one was found in the printed sample, but it is also a characteristic peak of the β form (Redenti et al., 1999). The characteristic peaks of PRX monohydrate appear at 1465 cm^{-1} and 1401 cm^{-1}, but neither was found in the printed films. The following peaks found in the printed films all correspond to the β form of PRX. The shifted medium-strong band at 1635 cm^{-1} and the strong band at the 1302 cm^{-1} regions are attributed to amide I and amide III. The shifted peaks at 831–730 cm^{-1} correspond to the δCH and ring modes. The medium and weak bands at 687 cm^{-1} and 653 cm^{-1} are attributed to amide V (Redenti et al., 1999; Adibkia et al., 2007; Taddei et al., 2001). The findings show that the PRX in the pure nanoPRX and the printed films are of β form, indicating that the manufacturing process did not affect the solid-state of the drug.

4.3.2. Raman spectroscopy

The different polymorphic forms of PRX were investigated in pure nanoPRX, PRX monohydrate, and the prepared films of the different printing inks by Raman spectroscopy. The Raman spectra were plotted

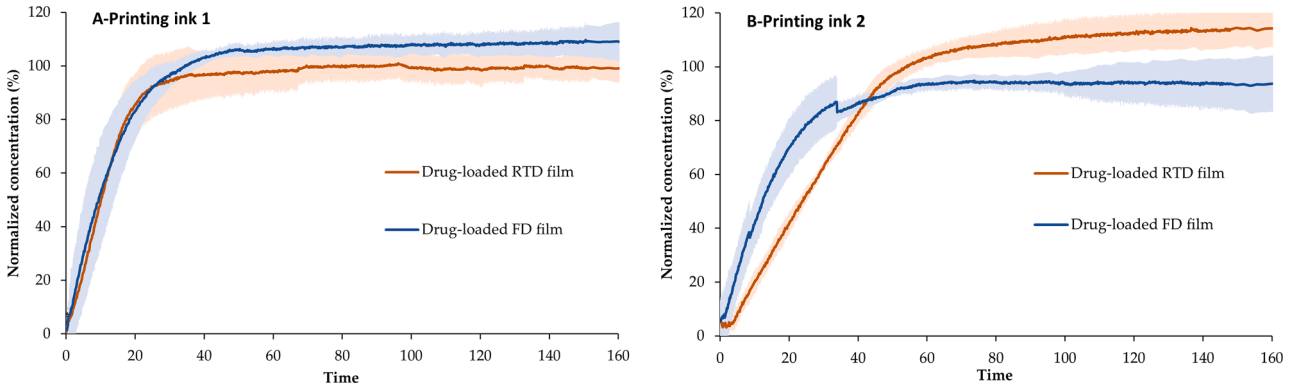

Fig. 6. Dissolution profile of semi-solid extrusion 3D printed, both room temperature-dried (RTD) and freeze-dried (FD) nanoPRX films of printing ink (PI) 1 and 2.

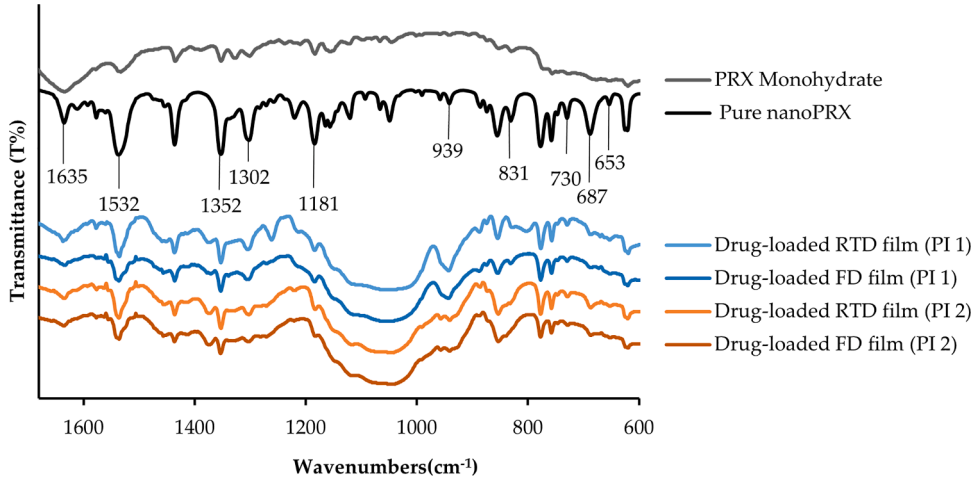

Fig. 7. Attenuated total reflectance Fourier transform infrared spectra of PRX monohydrate, pure nanoPRX, and room temperature-dried (RTD) and freeze-dried (FD) drug-loaded films prepared from printing inks (PI) 1 and 2.

from 1700 cm^{-1} to 1200 cm^{-1} to show the characteristic peaks. The characteristic peaks of PRX monohydrate should appear at 1464 cm^{-1} and 1397 cm^{-1} (Redenti et al., 1999), corresponding to the amide II attribution seen in Fig. A.6. The α form of PRX should present an amide II attribution to the Raman shift at 1543 cm^{-1}. In Fig. 8, pure nanoPRX and RTD and FD samples of printing inks 1 and 2 are visualized. None of the aforementioned peaks are found. The characteristic strong band shift for the β form of PRX is present at 1521 cm^{-1} (Redenti et al., 1999; Adibkia et al., 2007). The absence of the characteristic peaks for PRX monohydrate and PRX form α and the presence of the form β characteristic peak in pure nanoPRX and all films prepared from both printing inks confirms the ATR-FTIR findings that the solid-state of the drug has

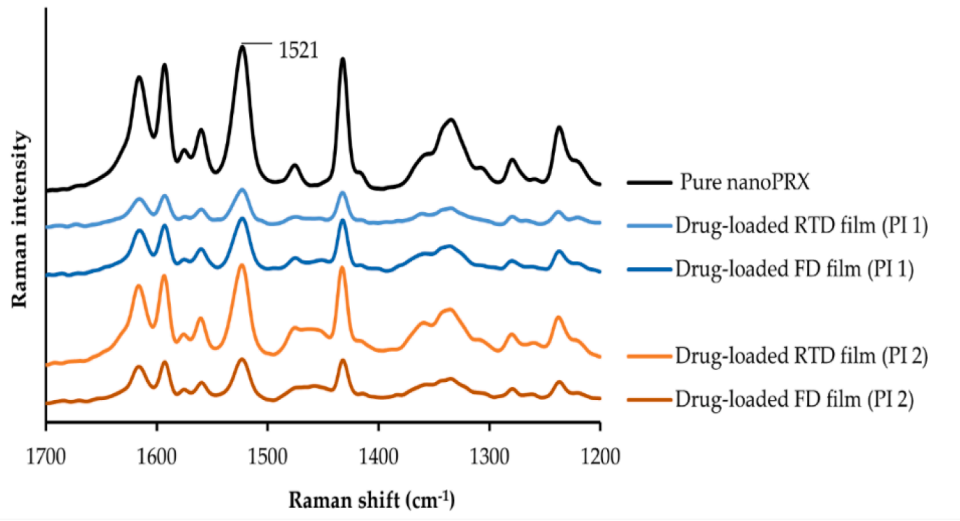

Fig. 8. Raman spectra of pure nanoPRX and room temperature-dried (RTD) and freeze-dried (FD) drug-loaded films of printing inks (PI) 1 and 2.

not changed form during formulating.

4.3.3. X-ray powder diffraction

The XRPD diffractograms of pure nanoPRX, and the RTD and FD drug-loaded printed films obtained from printing inks 1 and 2 are shown in Fig. 9. The obtained XRPD patterns in all printed films were similar to that of the pure nanoPRX. This indicates that no changes were observed in the drug's solid-state, confirming that the original solid-state form of nanoPRX has not changed during the preparation process. This further confirms the findings by ATR-FTIR and Raman analysis. The obtained XRPD peaks from printing ink 1 films were slightly lower in intensity and featured peak broadening compared to pure nanoPRX and printing ink 2 films. This broadening suggests decreasing crystallite size of the drug dispersed in the polymer with an increase in the polymer-to-drug ratio (Sandeep et al., 2018).

4.4. Stability study

The ATR-FTIR absorbance bands and the Raman peaks measured at one month after printing were identical to those obtained on the first day after printing, (Figs. A.5 and A.7). Furthermore, the dosage forms were measured with XRPD after three months of storage and the obtained peaks indicate that the nanoPRX was in its unchanged form. A slight shift is observed in FD films of printing ink 1 (Fig. A.8). The obtained results indicate that the nanosized PRX is stable and unchanged in the prepared dosage forms for at least three months.

5. Conclusions

Oral thin films containing therapeutic doses of CESS®-produced nanoPRX particles were successfully prepared utilizing SSE 3D printing. This study's primary aim was to stabilize the nanoPRX in an aqueous solution (ink base) and to maintain its original form throughout the manufacturing process. From the DLS results, Tylopur-605 was found to be a superior stabilizer and was chosen for suspension preparation. Suspension alone cannot be SSE 3D printed, hence an HPMC-based and an HPC-based aqueous polymer dispersion were prepared and combined with the drug suspension by microfluidic mixing to obtain two different printing inks. Printing ink 1 showed the ease of manufacturing, and the corresponding thin films exhibited fast disintegration, dissolution rate, and appropriate mechanical properties, despite being harder and more brittle than films prepared from printing ink 2. The correlation between the designed size and obtained drug amount was high ($R^2 = 0.9965$), proving the second aim of the study that personalized doses can be obtained by altering the area of the designed film. In conclusion, printing ink 1 was preferred over printing ink 2. In addition, two different drying methods were compared. The freeze-drying method expedited the drying from 24 h to 15 h when compared to ambient conditions. More importantly, freeze-drying improved the films' disintegration and dissolution. Extensive solid-state analysis was conducted to investigate the drug's polymorphic form. The studies confirmed that the prepared thin films contained nanoPRX in their original form and that the dosage form was stable for at least three months after printing. This study proves the concept of SSE 3D printing nanoformed particles to obtain personalized doses close to the point of care. The findings in this study can be utilized for other poorly water-soluble drugs in need of dose personalization to improve treatment outcomes, particularly in the pediatric and geriatric populations.

Work division between the two parties

Åbo Akademi University (ÅAU): Prepared the printing inks and conducted SSE 3D printing. The following analysis was performed by this party: DLS, TEM, rheology, mechanical strength, moisture content, drug content, disintegration, and solid-state characterization such as DSC, ATR-FTIR, and Raman spectroscopy. The first draft of the manuscript was written by this party.

Nanoform: Provided NanoPRX for the study. The following analysis was performed by this party: X-ray powder diffraction, *in vitro* dissolution, and scanning electron microscopy. Reviewing and editing of the manuscript were performed by this party.

CRediT authorship contribution statement

Rathna Mathiyalagan: Conceptualization, Methodology, Investigation, Writing – original draft, Visualization. **Erica Sjöholm:** Conceptualization, Methodology, Supervision, Investigation, Writing – original draft, Visualization. **Sajana Manandhar:** Methodology, Investigation, Writing – review & editing. **Satu Lakio:** Conceptualization, Methodology, Writing – review & editing. **Jessica M. Rosenholm:** Supervision, Writing – review & editing, Funding acquisition. **Martti Kaasalainen:** Conceptualization, Methodology, Supervision, Investigation, Writing – review & editing. **Xiaoju Wang:** Conceptualization, Methodology, Supervision, Investigation, Writing – review & editing, Project administration. **Niklas Sandler:** Conceptualization, Funding acquisition.

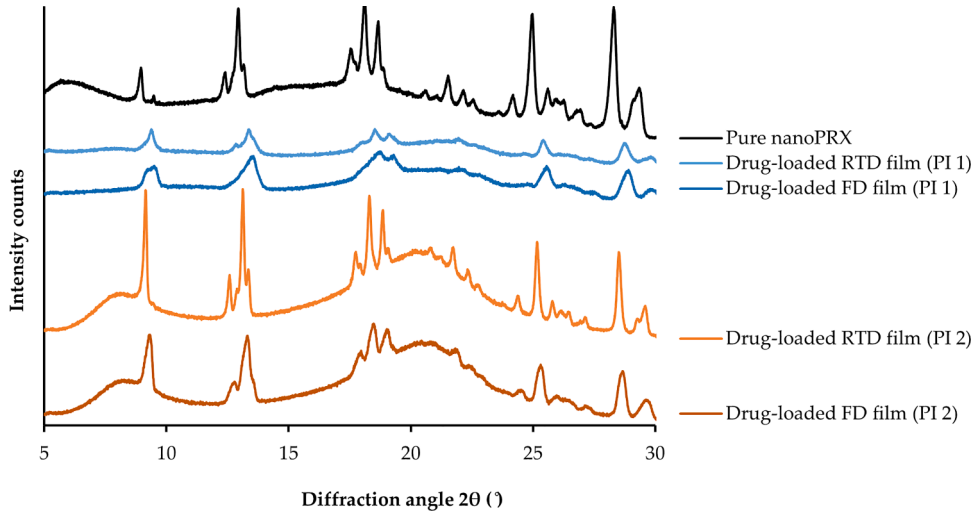

Fig. 9. X-ray powder diffraction pattern of pure nanoformed piroxicam (nanoPRX) and room temperature-dried (RTD) and freeze-dried (FD) nanoPRX-containing printed films printed with printing ink (PI) 1 and 2.

Declaration of Competing Interest

The authors declare that they have no known competing financial interests or personal relationships that could have appeared to influence the work reported in this paper.

Data availability

Data will be made available on request.

Acknowledgments

We thankfully acknowledge Dhayakumar Rajan Prakash for contributing to the microfluidic mixing process and Luyao Wang for performing the TEM study.

Funding

This research study was a collaborative project between ÅAU and Nanoform Finland Plc. Nanoform Finland Plc partly covered the salary of Rathna Mathiyalagan and Erica Sjöholm. Other funding sources we wish to acknowledge include the Academy of Finland (333158), the European regional development fund (ERDF) for the project 'AMBio-Pharma' (Centre for Additive Manufacturing for Life Science and Pharmaceutical Industry, project code A77805), and the Sigrid Jusélius Foundation (Finland) for their funds for research at ÅAU.

Supplementary materials

Supplementary material associated with this article can be found, in the online version, at doi:10.1016/j.ejps.2023.106497.

References

Adibkia, K., Shadbad, M.R.S., Nokhodchi, A., Javadzedeh, A., Barzegar-Jalali, M., Barar, J., Mohammadi, G., Omidi, Y., 2007. Piroxicam nanoparticles for ocular delivery: physicochemical characterization and implementation in endotoxin-induced uveitis. J. Drug Target. 15, 407–416. https://doi.org/10.1080/10611860701453125.

Alderman, D.A., 1984. A review of cellulose ethers in hydrophilic matrixes for oral controlled-release dosage forms. Int. J. Pharm. Technol. Prod. Manuf. 5.

Aminuddin, M., Nazim, U., Ahmad, I., 2011. Photo- and thermal degradation of piroxicam in aqueous solution. Indian J. Pharm. Sci. 73, 387–391. https://doi.org/10.4103/0250-474X.95615.

Bordner, J., Richards, J.A., Weeks, P., Whipple, E.B., 1984. Piroxicam monohydrate: a zwitterionic form, C15H13N3O4S.H2O. Acta Crystallogr. Sect. C. 40, 989–990. https://doi.org/10.1107/S0108270184006521.

Chou, P.Y., Chou, Y.C., Lai, Y.H., Lin, Y.T., Lu, C.J., Liu, S.J., 2021. Fabrication of drug-eluting nano-hydroxylapatite filled polycaprolactone nanocomposites using solution-extrusion 3d printing technique. Polymers (Basel) 13, 1–13. https://doi.org/10.3390/polym13030318.

Clayton, K.N., Salameh, J.W., Wereley, S.T., Kinzer-Ursem, T.L., 2016. Physical characterization of nanoparticle size and surface modification using particle scattering diffusometry. Biomicrofluidics 10, 1–14. https://doi.org/10.1063/1.4962992.

Danaei, M., Dehghankhold, M., Ataei, S., Hasanzadeh Davarani, F., Javanmard, R., Dokhani, A., Khorasani, S., Mozafari, M.R., 2018. Impact of particle size and polydispersity index on the clinical applications of lipidic nanocarrier systems. Pharmaceutics 10, 1–17. https://doi.org/10.3390/pharmaceutics10020057.

Duan, B., Kapetanovic, E., Hockaday, L.A., Butcher, J.T., 2014. Three-dimensional printed trileaflet valve conduits using biological hydrogels and human valve interstitial cells. Acta Biomater. 10, 1836–1846. https://doi.org/10.1016/j.actbio.2013.12.005.

Eisenstein, M., 2015. First 3D-printed pill. Nat. Biotechnol. 22, 1014. https://doi.org/10.1038/nbt1015-1014a.

Esfandi, E., Ramezani, V., Vatanara, A., Najafabadi, A.R., Hadipour Moghaddam, S.P., 2014. Clarithromycin dissolution enhancement by preparation of aqueous nanosuspensions using sonoprecipitation technique. Iran. J. Pharm. Res. 13, 809–818.

Germini, G., Peltonen, L., 2021. 3D printing of drug nanocrystals for film formulations. Molecules 26, 1–12. https://doi.org/10.3390/molecules26133941.

Hackley, V.A., Clogston, J.D., 2005. Measuring the size of nanoparticles in aqueous media using batch-mode dynamic light scattering NIST-NCL joint assay protocol, PCC-1 version 1.2. Natl. Inst. Stand. Technol. 1200, 1–17. https://doi.org/10.6028/NIST.SP.1200-6.

Hiremath, P., Nuguru, K., Agrahari, V., 2018. Material Attributes and Their Impact on Wet Granulation Process Performance. Elsevier Inc. https://doi.org/10.1016/B978-0-12-810460-6.00012-9

Jamróz, W., Szafraniec-Szczęsny, J., Kurek, M., Jachowicz, R., 2018. 3D printing in pharmaceutical and medical applications – recent achievements and challenges. Pharm. Res. 35 https://doi.org/10.1007/s11095-018-2454-x.

Kaasalainen, M., Aseyev, V., von Haartman, E., Karaman, D.Ş., Mäkilä, E., Tenhu, H., Rosenholm, J., Salonen, J., 2017. Size, stability, and porosity of mesoporous nanoparticles characterized with light scattering. Nanoscale Res. Lett. 12 https://doi.org/10.1186/s11671-017-1853-y.

Kompella, U.B., 1999. Drug delivery applications of supercritical fluid technology. IDrugs 2, 33–34. http://europepmc.org/abstract/MED/16180167.

Lakio, S., Sandler, N., 2020. Nanoparticle engineering: revolutionising oral drug development & delivery. ONdrugDelivery 2020, 26–29.

Lir, I., Haber, M., Dodiuk-Kenig, H., 2007. Skin surface model material as a substrate for adhesion-to-skin testing. J. Adhes. Sci. Technol. 21, 1497–1512. https://doi.org/10.1163/156856107782844783.

Liu, J., Tagami, T., Ozeki, T., 2020. Fabrication of 3D-printed fish-gelatin-based polymer hydrogel patches for local delivery of pegylated liposomal doxorubicin. Mar. Drugs 18. https://doi.org/10.3390/md18060325.

Loftsson, T., Brewster, M.E., 2010. Pharmaceutical applications of cyclodextrins: basic science and product development. J. Pharm. Pharmacol. 62, 1607–1621. https://doi.org/10.1111/j.2042-7158.2010.01030.x.

Maruyama, S., Ooshima, H., 2001. Mechanism of the solvent-mediated transformation of taltirelin polymorphs promoted by methanol. Chem. Eng. J. 81, 1–7. https://doi.org/10.1016/S1385-8947(00)00193-5.

Mirdamadian, S.Z., Varshosaz, J., Minaiyan, M., Taheri, A., 2022. 3D printed tablets containing oxaliplatin loaded alginate nanoparticles for colon cancer targeted delivery. An in vitro/in vivo study. Int. J. Biol. Macromol. 205, 90–109. https://doi.org/10.1016/j.ijbiomac.2022.02.080.

Mohammed, N.N., Majumdar, S., Singh, A., Deng, W., Murthy, N.S., Pinto, E., Tewari, D., Durig, T., Repka, M.A., 2012. Klucel^{TM} EF and ELF polymers for immediate-release oral dosage forms prepared by melt extrusion technology. AAPS PharmSciTech 13, 1158–1169. https://doi.org/10.1208/s12249-012-9834-z.

Möschwitzer, J., Achleitner, G., Pomper, H., Müller, R.H., 2004. Development of an intravenously injectable chemically stable aqueous omeprazole formulation using nanosuspension technology. Eur. J. Pharm. Biopharm. 58, 615–619. https://doi.org/10.1016/j.ejpb.2004.03.022.

Nair, A.B., Kumria, R., Harsha, S., Attimarad, M., Al-Dhubiab, B.E., Alhaider, I.A., 2013. In vitro techniques to evaluate buccal films. J. Control. Release 166, 10–21. https://doi.org/10.1016/j.jconrel.2012.11.019.

Nallan, H.C., Sadie, J.A., Kitsomboonloha, R., Volkman, S.K., Subramanian, V., 2014. Systematic design of jettable nanoparticle-based inkjet inks: rheology, acoustics, and jettability. Langmuir 30, 13470–13477. https://doi.org/10.1021/la502903y.

Öblom, H., Sjöholm, E., Rautamo, M., Sandler, N., 2019. Towards printed pediatric medicines in hospital pharmacies: comparison of 2D and 3D-printed orodispersible warfarin films with conventional oral powders in unit dose sachets. Pharmaceutics 11. https://doi.org/10.3390/pharmaceutics11070334.

Panraksa, P., Udomsom, S., Rachtanapun, P., Chittasupho, C., Ruksiriwanich, W., Jantrawut, P., 2020. Hydroxypropyl methylcellulose e15: a hydrophilic polymer for fabrication of orodispersible film using syringe extrusion 3D printer. Polymers (Basel) 12, 1–14. https://doi.org/10.3390/polym12112666.

Pechová, V., Gajdziok, J., Muselík, J., Vetchý, D., 2018. Development of orodispersible films containing benzydamine hydrochloride using a modified solvent casting method. AAPS PharmSciTech 19, 2509–2518. https://doi.org/10.1208/s12249-018-1088-y.

Pessi, J., Lassila, I., Meriläinen, A., Räikkönen, H., Hæggström, E., Yliruusi, J., 2016. Controlled expansion of supercritical solution: a robust method to produce pure drug nanoparticles with narrow size-distribution. J. Pharm. Sci. 105, 2293–2297. https://doi.org/10.1016/j.xphs.2016.05.022.

Redenti, E., Zanol, M., Ventura, P., Fronza, G., Comotti, A., Taddei, P., Bertoluzza, A., 1999. Raman and solid state 13C-NMR investigation of the structure of the 1: 1 amorphous piroxicam: β-Cyclodextrin inclusion compound. Biospectroscopy 5, 243–251. https://doi.org/10.1002/(SICI)1520-6343(1999)5:4<243::AID-BSPY5>3.0.CO;2-C.

Reis, N., Derby, B., 2003. Inkjet printing of highly loaded particulate suspensions. MRS Bull. 28, 815–818. http://cat.inist.fr/?aModele=afficheN&cpsidt=15290250.

Sakho, E.H.M., Allahyari, E., Oluwafemi, O.S., Thomas, S., Kalarikkal, N., 2017. Dynamic light scattering (DLS). Therm. Rheol. Meas. Tech. Nanomater. Charact. 3, 37–49. https://doi.org/10.1016/B978-0-323-46139-9.00002-5.

Sandeep, P., Aditya D, K., Avinash, C.LA, C, P., K, V., 2018. In vitro dissolution studies on naproxen-PVP nanoformulations show enhanced oral bioavailability of naproxen. Int. J. Med. Nano Res. 5, 1–9. https://doi.org/10.23937/2378-3664/1410023.

Savjani, K.T., Gajjar, A.K., Savjani, J.K., 2012. Drug solubility: importance and enhancement techniques. ISRN Pharm. 2012, 1–10. https://doi.org/10.5402/2012/195727.

Schmidt, L.M., dos Santos, J., de Oliveira, T.V., Funk, N.L., Petzhold, C.L., Benvenutti, E. V., Deon, M., Beck, R.C.R., 2022. Drug-loaded mesoporous silica on carboxymethyl cellulose hydrogel: development of innovative 3D printed hydrophilic films. Int. J. Pharm. 620, 121750 https://doi.org/10.1016/j.ijpharm.2022.121750.

Shahrubudin, N., Lee, T.C., Ramlan, R., 2019. An overview on 3D printing technology: technological, materials, and applications. Procedia Manuf. 35, 1286–1296. https://doi.org/10.1016/j.promfg.2019.06.089.

Sheth, A.R., Lubach, J.W., Munson, E.J., Muller, F.X., Grant, D.J.W., 2005. Mechanochromism of piroxicam accompanied by intermolecular proton transfer probed by spectroscopic methods and solid-phase changes. J. Am. Chem. Soc. 127, 6641–6651. https://doi.org/10.1021/ja045823t.

Shohin, I.E., Kulinich, J.I., Ramenskaya, G.V., Abrahamsson, B., Kopp, S., Langguth, P., Polli, J.E., Shah, V.P., Groot, D.W., Barends, D.M., Dressman, J.B., 2014. Biowaiver monographs for immediate release solid oral dosage forms: piroxicam. J. Pharm. Sci. 103, 367–377. https://doi.org/10.1002/jps.23799.

Sjöholm, E., Mathiyalagan, R., Prakash, D.R., Lindfors, L., Wang, Q., Wang, X., Ojala, S., Sandler, N., 2020. 3D-printed veterinary dosage forms—a comparative study of three semi-solid extrusion 3D printers. Pharmaceutics 12, 1–26. https://doi.org/10.3390/pharmaceutics12121239.

Sjöholm, E., Mathiyalagan, R., Wang, X., Sandler, N., 2022. Compounding tailored veterinary chewable tablets close to the point-of-care by means of 3D printing. Pharmaceutics 14, 1339. https://doi.org/10.3390/pharmaceutics14071339.

Sjöholm, E., Sandler, N., 2019. Additive manufacturing of personalized orodispersible warfarin films. Int. J. Pharm. 564, 117–123. https://doi.org/10.1016/j.ijpharm.2019.04.018.

Tablets, in: Ph. Eur, 11.0, Council of Europe, Strasbourg, France, 2018: pp. 1004–1006.

Disintegration of Tablets and Capsules, 2022. Council of Europe, Strasbourg, France, pp. 345–347. Ph. Eur, 11.0.

Taddei, P., Torreggiani, A., Simoni, R., 2001. Influence of environment on piroxicam polymorphism: vibrational spectroscopic study. Biopolym. - Biospectroscopy Sect. 62, 68–78. https://doi.org/10.1002/1097-0282(2001)62:1<68::AID-BIP80>3.0.CO;2-X.

The Dow Chemical Company, METHOCEL Cellulose Ethers Technical Handbook, U.S.A., 2002. Form No. 192-01062-0902 AMS.

Dissolution Test for Solid Dosage Forms, 2023. Council of Europe, Strasbourg, France, pp. 348–354. Ph. Eur, 11.0.

Topsakal, A., Midha, S., Yuca, E., Tukay, A., Sasmazel, H.T., Kalaskar, D.M., Gunduz, O., 2021. Study on the cytocompatibility, mechanical and antimicrobial properties of 3D printed composite scaffolds based on PVA/Gold nanoparticles (AuNP)/ Ampicillin (AMP) for bone tissue engineering. Mater. Today Commun. 28, 102458 https://doi.org/10.1016/j.mtcomm.2021.102458.

Trenfield, S.J., Awad, A., Goyanes, A., Gaisford, S., Basit, A.W., 2018. 3D printing pharmaceuticals: drug development to frontline care. Trends Pharmacol. Sci. 39, 440–451. https://doi.org/10.1016/j.tips.2018.02.006.

Vaz, V.M., Kumar, L., 2021. 3D printing as a promising tool in personalized medicine. AAPS PharmSciTech 22. https://doi.org/10.1208/s12249-020-01905-8.

Viridén, A., Wittgren, B., Andersson, T., Larsson, A., 2009. The effect of chemical heterogeneity of HPMC on polymer release from matrix tablets. Eur. J. Pharm. Sci. 36, 392–400. https://doi.org/10.1016/j.ejps.2008.11.003.

Wang, R., Tao, J., Du, K., Wang, Y., Ge, B., Li, F., Liu, W., Wu, L., Liu, H., Zhang, Y., Yao, Y., Duan, X., 2018. Transmission electron microscopy. Springer Tracts Mod. Phys. 272, 69–203. https://doi.org/10.1007/978-981-13-0454-5_3.

Yang, Y., Bi, V., Dürig, T., Ingredients, A.S., 2016. The impact of hydroxypropyl methylcellulose and methylcellulose molecular weight and degree of substitution on crystallization inhibition of felodipine in aqueous media. Pharm. Technol. Rep. 04, 1–5.

Y. Zhang, J. Zhang, R. Thakkar, A.R. Pillai, J. Wang, M. Maniruzzaman, Functions of magnetic nanoparticles in selective laser sintering (SLS) 3D printing of pharmaceutical dosage forms, (2021) 1–29. 10.26434/chemrxiv.13925177.v1.